

A new sampling methodology for defining heterogeneous subsets of samples for training image segmentation algorithms

Matheus Viana da Silva,¹ Natália de Carvalho Santos,² Julie Ouellette,^{3,4} Baptiste Lacoste,^{3,4} and Cesar H. Comin^{1,*}

¹*Department of Computer Science, Federal University of São Carlos, São Carlos, SP, Brazil*

²*São Carlos Institute of Physics, University of São Paulo, São Carlos, SP, Brazil*

³*Department of Cellular and Molecular Medicine,*

Faculty of Medicine, University of Ottawa, Ottawa, ON, Canada

⁴*Neuroscience Program, Ottawa Hospital Research Institute, Ottawa, ON, Canada*

(Dated: December 5, 2023)

Creating a dataset for training supervised machine learning algorithms can be a demanding task. This is especially true for medical image segmentation since one or more specialists are usually required for image annotation, and creating ground truth labels for just a single image can take up to several hours. In addition, it is paramount that the annotated samples represent well the different conditions that might affect the imaged tissues as well as possible changes in the image acquisition process. This can only be achieved by considering samples that are typical in the dataset as well as atypical, or even outlier, samples. We introduce a new sampling methodology for selecting relevant images from a large dataset in a way that evenly considers both prototypical as well as atypical samples. The methodology involves the generation of a uniform grid from a feature space representing the samples, which is then used for randomly drawing relevant images. The selected images provide a uniform covering of the original dataset, and thus define a heterogeneous set of images that can be annotated and used for training supervised segmentation algorithms. We provide a case example by creating a dataset containing a representative set of blood vessel microscopy images selected from a larger dataset containing thousands of images. The dataset, which we call VessMAP, is being made available online to aid the development of new blood vessel segmentation algorithms.

Keywords: dataset sampling, efficient annotation, segmentation, blood vessel

I. INTRODUCTION

Recent developments in neural networks led to unprecedented results in image classification [1–4], object detection [5–7] and image segmentation [5, 8, 9]. Neural networks shifted the focus from feature engineering to a more data-centric approach, where network models can approximate highly complex functions provided the model has enough capacity and the dataset is sufficiently representative [10].

The performance of neural networks has dominantly been measured using metrics such as classification or segmentation accuracy, precision, recall, and the area under the ROC curve. However, recent studies have shown the dangers of only considering such globally-averaged metrics [11–13] that provide only an aggregated, summarized, view of the performance of machine learning algorithms on datasets with sometimes millions of images. Such an approach may hide important biases of the model [13]. For instance, for medical images, a 95% accuracy is usually considered a good performance. But what about the remaining 5%? It is usually unrealistic to expect models to reach 100% accuracy, but the samples that are not correctly processed by a neural network may hide important biases of the model. These concerns led to the definition of new approaches and metrics that can aid the interpretation of black box models [14].

For the task of segmentation in medical images, which is the focus, but not the only application of our study, the detection of relevant structures is usually only the first step of a more elaborate procedure for measuring relevant properties such as size [15], regularity [16], length [17, 18], and curvature [18, 19] of the imaged structures. Therefore, systematic segmentation mistakes might lead to undetected errors when characterizing samples for clinical diagnoses [20] and research purposes [11]. An important cause of such systematic errors can be the presence of samples having characteristics that occur with low frequency in a dataset. This can happen due to additional, unexpected, noise during image acquisition, variations in tissue staining, image artifacts, or even the presence of structures that are anatomically different than what was expected. Assuming for illustration purposes that the data is normally distributed, a machine learning model having good performance around the peak of the distribution will tend to have good average accuracy measured for the whole dataset, even if it cannot correctly classify or segment images that are around the tail of the distribution [21], which might be important for downstream analyses. Notice that this discussion does not necessarily only involves outlier images, but any image occurring with low probability.

Here we argue that a machine learning model should have good performance, or even be directly optimized, on both prototypical and atypical samples. This focus can lead to models that are more robust to samples located in a sparsely populated region of the feature space of the

* Corresponding author: chcomin@gmail.com

dataset. In addition, it might also lead to models that generalize better to out-of-distribution samples as well as to new datasets. We develop a simple and intuitive sampling methodology to select a subset of images from a dataset representing, as best as possible, a uniform coverage of the feature space of all the samples. This subset can be used for measuring the homogeneity of the performance of the model on highly distinct samples. It can also be used for identifying regions in the feature space where the model does not perform well.

We focus on applying the method to the important problem of selecting relevant samples for ground truth mask annotation for training segmentation algorithms. For medical images, manually annotating masks can be very time consuming and usually requires skilled workers or specialists. Therefore, when many samples are available for annotation, it is interesting to select an optimal subset of samples that leads to a model that is also expected to perform well on the whole dataset. To this end, we present a case example of selecting an appropriate subset of samples from a blood vessel dataset containing 2637 images. We show that the selected samples uniformly cover different properties of the images and thus represent a rich set of samples that can be annotated and used for training a segmentation algorithm for processing the whole dataset.

A concept that is similar to the developed methodology is the so-called *coreset* [22]. The aim of a coresnet is to select a subset of samples that can optimally represent the whole dataset. Many different methodologies and criteria were developed for defining relevant coresets [22–24]. Indeed, the subset defined by our methodology can be associated with a coresnet, but in our case, the aim of the generated subset and the approach used differs markedly from the usual definition of a coresnet. The aim of our methodology is not focused on accurately representing the underlying distribution of the data, or on preserving the accuracy of a machine learning algorithm, but on providing a relevant dataset for training machine learning algorithms while avoiding the underrepresentation of atypical samples. In addition, many coresnet methodologies use a surrogate neural network to estimate latent features or to estimate a degree of uncertainty about each sample, while our methodology is more general in the sense that any set of features obtained from the samples can be used. Those can even be specific features such as image contrast and average intensity. Furthermore, many related studies consider a similarity metric for selecting relevant samples [23, 24], which is a degenerate metric and therefore cannot provide a full representation of the data distribution.

II. METHODOLOGY

The sampling methodology proposed in this work can be divided into three steps: (a) dataset mapping to an n -dimensional feature space, (b) generation of a discrete

representation of the feature space, and (c) selection of points from the feature space representation. We explain each of these steps in the following subsections ¹.

A. Dataset mapping

Given a dataset $D = \{\delta_1, \delta_2, \dots, \delta_n\}$ with n samples, and a function $f : \delta_i \rightarrow \vec{p}_i$ that maps a sample δ_i to a vector \vec{p}_i with dimension d , the new dataset mapped to a feature space can be represented as an $n \times d$ matrix, which we call D_{mapped} . Each line of this matrix therefore represents the features of a sample $f(\delta_i)$. Figure 1 illustrates this procedure for a dataset D . Each sample in D (Figure 1(a)) is mapped to a point in the new feature space (Figure 1(b)).

There are many different approaches for defining $f(\delta_i)$. For example, if D is a set of images, we can map each image using a combination of relevant features, such as image contrast or signal-to-noise ratio. Feature mapping can also be achieved through a prior unsupervised or semi-supervised segmentation of the objects in the images. In this case, features such as object area or elongation can be used. Supervised learning can also be used to map the images to a new feature space. In this scenario, instead of mapping D through handcrafted features, the features learned by a supervised segmentation algorithm, such as a neural network, can be used. In Section III we present an example with a mapping function defined as a combination of global image features and handcrafted features from semi-supervised segmentation.

B. Feature space discretization

The second step of the methodology is to define a regular grid in the feature space and to translate each data point to the nearest point in this grid. It is useful to first normalize the values of D_{mapped} to remove differences in the scale of the features. In this work, we used z-score normalization, but other normalizations can be used. After normalizing D_{mapped} , we proceed to resample the mapped values to a discrete grid. This is done by defining a scale ν that sets the size of each grid cell and calculating

$$D_{\text{grid}} = \text{floor} \left(\frac{D_{\text{mapped}}}{\nu} \right), \quad (1)$$

where *floor* is the floor function. As shown in Figure 1(c), this operation ensures that each value of D_{grid} lies within a regular grid. Note that, as a consequence of undersampling, we expect multiple data points to fall in

¹ https://github.com/matheus-viana/heterogeneous_sampling

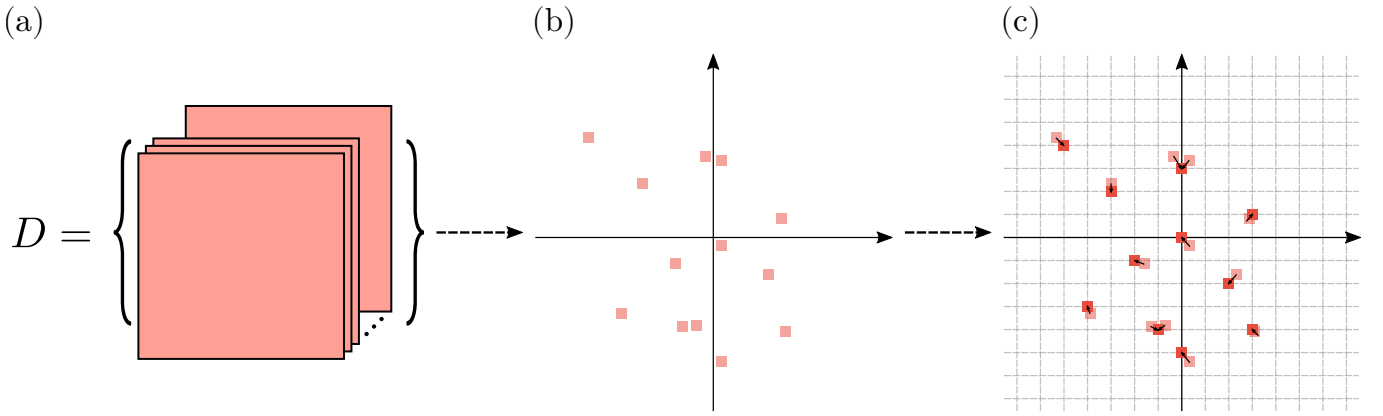


FIG. 1. Representation of the mapping procedure applied to a set D of samples, followed by the feature space discretization. Here, we consider D as a set of images. In this example, each image of D is mapped to a 2-d position in the new feature space (b). In (c), the mapped points (light-red points) are moved to a new position (red points) within a regular grid defined by Equation 1.

the same grid position, this is one of the key properties of the method that will allow a uniform sampling of the data.

After feature space discretization, we generate a sparse set of points representing an estimation of the possible values that can be obtained in the feature space. We call this set the *sampling set* of the feature space. As illustrated in Figure 2, this procedure works as follows. An n -dimensional discrete hypersphere S with radius r (in grid units) centered on each data point is defined (Figure 2(a)). This hypersphere is translated to each data point position. The union of the calculated hypersphere positions of all points (Figure 2(b)) defines the sampling set D_{sset} .

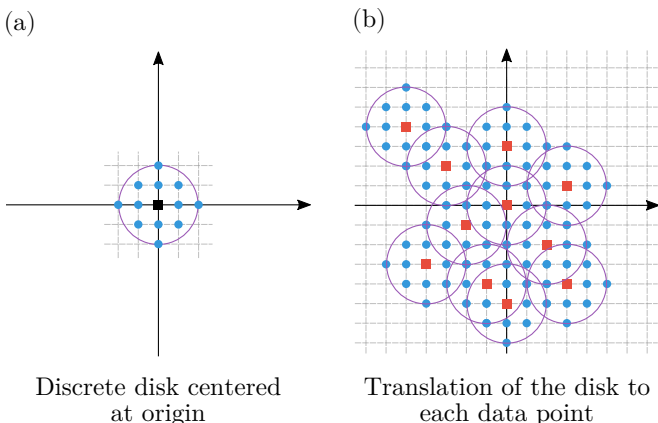


FIG. 2. Estimation of the feasible values of the feature space. In (a) we define a sparse hypersphere (depicted as a disk for visualization) as a set of uniformly distributed points. This disk is translated to the center of each point in D_{grid} (red points of (b)). The union of all hypersphere points defines D_{sset} .

Given that our algorithm operates over a discrete space, we expect repeated hypersphere points in D_{sset}

after translation. These repeated values account for important information regarding the spatial distribution of the points in D_{sset} and can be stored and used to sample the points in a non-uniform manner. Since the main goal of the methodology is to select heterogeneous subsets from the original data, which can optimally be done using a uniform distribution, we ignore repeated points in D_{sset} .

C. Uniform selection of samples

The last step consists of drawing a set of points from the sampling set D_{sset} . As illustrated in Figure 3, we draw from D_{sset} k points with uniform probability (green dots in Figure 3). For each point drawn, the closest data sample is identified using the Euclidean distance. If the same data sample is obtained more than once, a new point is drawn from D_{sset} until k unique data samples are obtained. The final set of data samples (orange stars in Figure 3) is represented as $D_{sampled}$.

As mentioned before, a uniform sampling of D_{sset} allows the selection of prototypical and atypical samples from the dataset with equal probability. Nevertheless, a single realization of the sampling may lead to distortions such as the selection of many samples at similar regions of the space or the creation of large regions with no samples selected. This is due to random fluctuations in the sampling process. To amend this, we define a metric called Farthest Unselected Point (FUS), that punishes sampled subsets with large gaps between the selected points.

Let $D_{sampled}$ be the set of sampled data points from D_{grid} , and $\neg D_{sampled}$ the set of points from D_{grid} that were not selected in the sampled subset. For each data point in $\neg D_{sampled}$, the Euclidean distance to the closest point in $D_{sampled}$ is obtained. The FUS metric is defined as the largest calculated distance among all points in $\neg D_{sampled}$. Sampled subsets leading to low values of

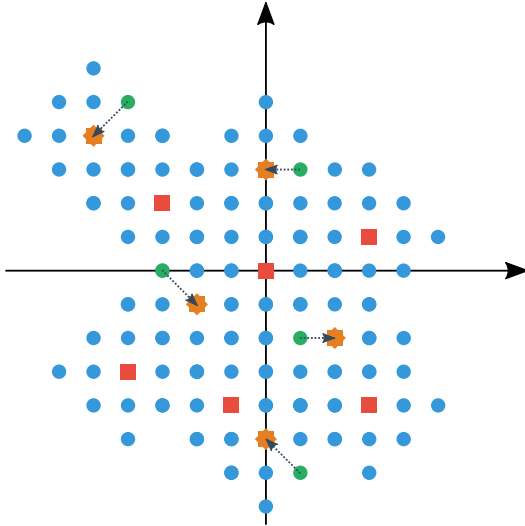


FIG. 3. Illustration of the proposed sampling protocol. k random points (green dots) are drawn from the sampling set D_{sset} (blue dots). The subset of sampled data points is defined by the data points that are closest to each drawn point (orange stars). Red squares represent the remaining data points that were not selected.

the FUS metric should be preferred, since it avoids the creation of large regions of the feature space with no samples. The metric is illustrated in Figure 4. In Figure 4(a), the farthest unselected point evidences a gap of sampled points in the upper right corner of the distribution. This gap is less pronounced in Figure 4(b), where the points are sampled more heterogeneously and unselected points are, in general, close to the sampled subset distribution. With that in mind, $D_{sampled}$ is given as the set with the lowest FUS amongst N sampled subsets. In our experiments, we find that $N \geq 1000$ covers a good amount of subset possibilities, but the optimal value of N may change depending on the dataset being studied.

To illustrate the potential of the methodology, Figure 5 shows a comparison between the usual approach for selecting a subset of the data, to simply draw images at random with equal probability from the dataset, and the selection of points using the presented method. Using uniform sampling, the points tend to be selected according to the underlying probability density function of the data, which is usually unknown. Thus, most of the selected points will tend to be located in denser regions of the feature space, which consequently biases the sampled subset towards the regions of the dataset with prototypical examples (Figure 5(a)). By drawing the subset of points using our methodology, the selected points will tend to cover the feature space more uniformly (Figure 5(b)).

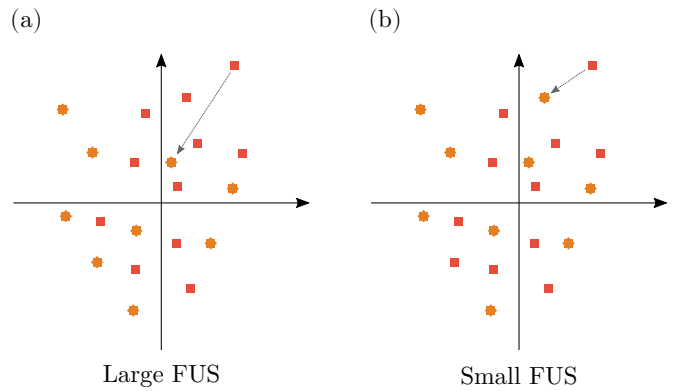


FIG. 4. An illustration of how minimizing the FUS metric also minimizes gaps between sampled points. In (a), a higher distance between unselected points (depicted as red squares) and sampled points (depicted as orange stars) indicates a large gap between sampled points. This behavior is less pronounced in (b), where a more heterogeneous subset was sampled.

III. CASE EXAMPLE – CREATING A DATASET FOR BLOOD VESSEL SEGMENTATION

To show the potential of the methodology, in this section we describe an application of the method on real data. We show how the method can aid in the selection of a heterogeneous set of samples that can then be used for training a supervised segmentation algorithm.

A. Blood vessel dataset

The dataset contains confocal microscopy images of mouse brain vasculature. The dataset has 2637 images having sizes from 1376×1104 to 2499×2005 pixels, totaling around 3.8GB of data. The images were acquired under different experimental conditions in different works published in the literature [25–27]. Conditions include control animals, animals that have suffered a deletion of chromosome 16p11.12, animals that have experienced sense deprivation or sense hyperarousal, samples from stroke regions, and also from different stages of mouse development.

The dataset is interesting because it has a considerable variety of characteristics of blood vessels. In addition, the images represent samples obtained from hundreds of different animals and experimental conditions. This makes it an excellent dataset for training machine learning algorithms for blood vessel segmentation. But training supervised algorithms requires the manual annotation of the blood vessels in a subset of the images.

After annotating a few samples, we estimated that each image in the dataset takes roughly 12 hours to fully annotate. Therefore, it is unfeasible to annotate the whole dataset. Thus, it is interesting to select relevant samples for annotation in order to train a machine learning

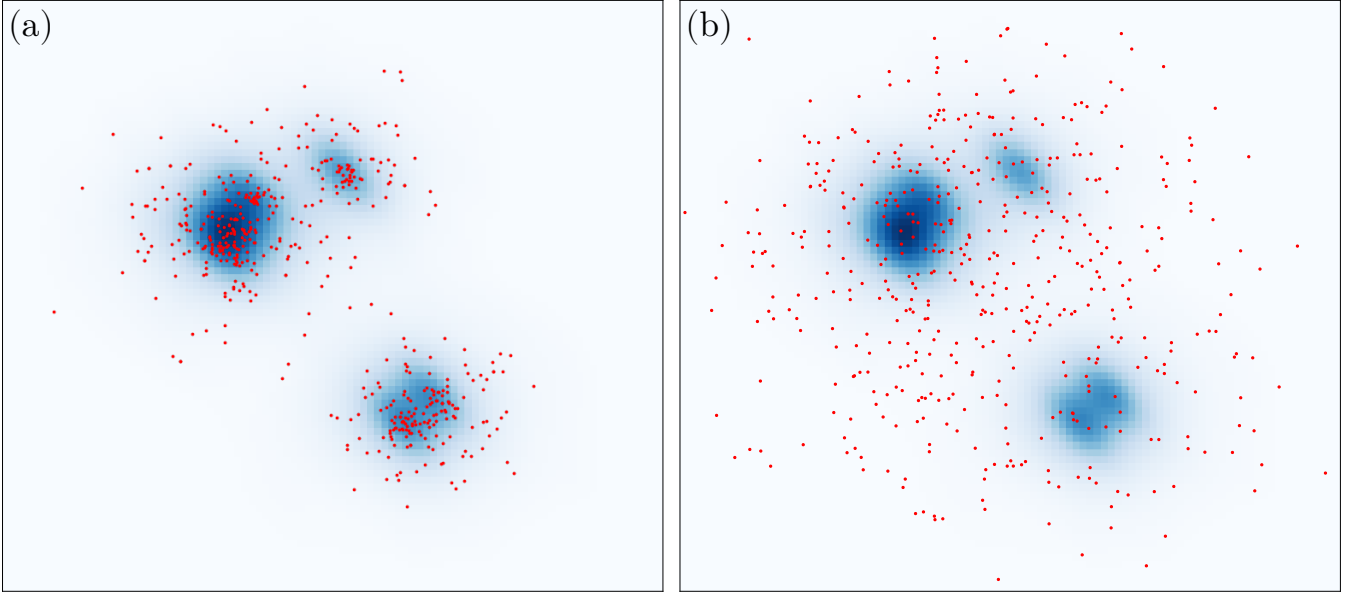


FIG. 5. Illustration of two sampling strategies. Red dots represent the sampled points. The background color represents the underlying probability density function of the data, with larger values having darker tones of blue. In (a), we have a typical example of uniformly drawing samples from a dataset, which leads to the selection of many samples that are similar to each other. In (b), the points are selected using the presented methodology. In this case, the sampled points are spread out and cover the feature space.

algorithm to segment the whole dataset. As mentioned before, this subset of samples should allow the training to occur without biases, that is, atypical samples should be well-represented so that the accuracy of the algorithm depends as little as possible on the properties of the images or the tissues under analysis. This means that it is important to select both prototypical and atypical samples for annotation.

Each image in the dataset may include illumination inhomogeneities, changes in contrast, different levels of noise, as well as blood vessels having distinct characteristics (e.g., caliber, tortuosity, etc). Thus, from the original dataset, we generated a new set of images, each having a size of 256×256 pixels. These smaller images were generated by extracting 256×256 regions from the original images. As shown in Figure 6, seven regions were extracted from each image. The seven regions were extracted in key areas of each image, with four windows in each of the corners of the image, a central window, and two windows at random positions. The latter two may overlap with the other windows. Windows that did not contain a satisfactory number of blood vessel segments were removed. The total size of the resulting dataset is 18279 images.

The extracted images were mapped to a feature space that was used for characterizing the samples. As mentioned in Section II A, image features can be calculated by processing labels obtained from semi-supervised segmentation. Since our dataset was used in previous works, each image has a respective segmentation that was obtained using a semi-supervised methodology. This

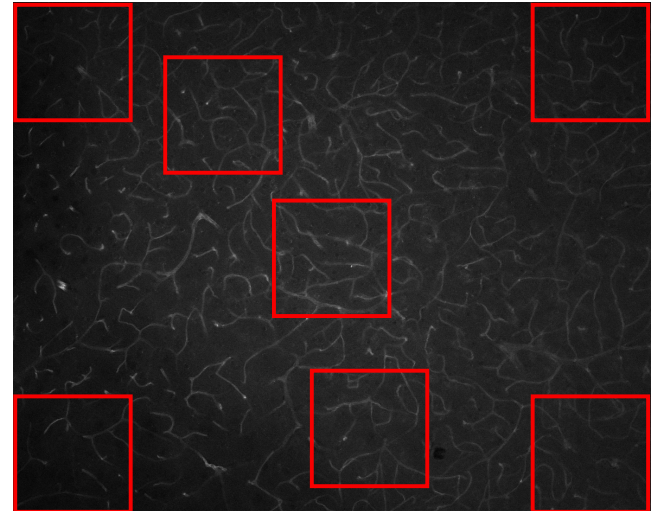


FIG. 6. An example of seven regions extracted from a single sample. The four corners along with the central region can capture most of the illumination inhomogeneities that may occur due to uneven illumination of the samples. Besides these five regions, two additional random regions are also drawn for each image.

methodology is based on the adaptive thresholding of the original images, where the threshold was selected manually for each image. The full details on the segmentation procedure are described in [18].

B. Metrics

The following features were used to characterize the samples: blood vessel contrast, level of Gaussian noise, blood vessel density, and medial line heterogeneity.

The blood vessel contrast is related to the average difference in intensity between the vessels and the background of the image. The greater the contrast, the easier it is to detect the vessels. It can be measured using the original image of the vessels and the respective thresholded image containing an estimation of the pixels belonging to the vessels. The contrast is calculated as

$$C = \frac{\bar{I}_v}{\bar{I}_f}, \quad (2)$$

where \bar{I}_v and \bar{I}_f are the mean intensities of, respectively, the pixels belonging to the blood vessels and the background of the image.

The signal-to-noise level of the images can be estimated in different ways. We investigated different definitions and used the method that was the most compatible with a visual inspection of the images. The method proposed in [28] was used. It assumes a noise with normal distribution and uses wavelets to identify the most likely standard deviation of the noise component. To prevent the method from capturing vessel variation, only the background of the image was used for the estimation.

Blood vessel density is defined as the total length of blood vessels in an image divided by the image area. To do this, we first apply a skeletonization algorithm to extract the medial lines of the vessels [29]. The total length of vessels is calculated as the sum of the arc-lengths of all vessel segments.

The last metric, which we call medial line heterogeneity, measures the illumination changes in the vessel lumen. To calculate this metric, we first blur the image using a gaussian filter with unit standard deviation to remove extreme values. The medial line heterogeneity is calculated as the standard deviation of the pixel values along the medial lines of this blurred image. The medial lines considered are the same ones used for the blood vessel density metric.

We observed that the medial line heterogeneity tends to be correlated with the average intensity of the blood vessels. In order to remove this dependency, the medial line heterogeneity as well as the average intensity of the medial lines was calculated for all images in the dataset. Then, a straight line fit $h_m = a*m + b$ was applied to the calculated values, where m is the average intensity and h_m is the expected medial line heterogeneity associated with m . Next, a normalized medial line heterogeneity was defined as $\tilde{h} = h - h_m$, where h is the medial line heterogeneity calculated for an image.

C. Generation of a diverse subset of samples for annotation

The four metrics described in the previous section were used for mapping the dataset to a 4-d feature space by applying the methodology detailed in Section II A. As mentioned before, the dataset contains 18279 images. Hence, the whole dataset was mapped to a 18279×4 matrix. In the feature space discretization step (Section II B), we used z-score normalization and a scale of $\nu = 10$. The hypersphere was generated with a radius equal to four times the grid space resolution. In the sampling step (Section II C), we used $N = 1000$ and chose the sampling solution that minimized the FUS metric. The sampled subset size contained $k = 100$ images. To avoid data leaking, an additional restriction that prevented the selection of samples from the same image was used.

The generated subset contains a heterogeneous set of samples that can be used for annotation. It is difficult to properly measure the heterogeneity of this subset because it would involve the estimation of the probability density function of the original data, which is not a trivial task and can be influenced by the choice of parameter values. But it is clear that the method must naturally lead to a uniform selection of the samples. This is so because the set D_{grid} (defined in Section II B) represents an estimation of the domain of the probability density function of the data, and this domain is being sampled uniformly.

One approach to illustrate the characteristics of the sampled images is displayed in Figure 7, which shows histograms of the four considered features for both the full dataset and the sampled subset. The histograms of individual features are not expected to be uniform since they represent a projection of the original data into one dimension. Still, it can be seen that the histograms of the sampled set tend to represent a slightly flattened version of the histograms of the original data, indicating that a larger priority is being given to atypical samples when compared to the original distribution.

A more robust way of visually checking the sampled subset is to visualize the data using Principal Component Analysis (PCA). Using PCA, the original 4-d data can be projected into 2-d with optimal preservation of the variance. Figure 8 shows the PCA projection of the data. The four plots included in the figure represent the same projection, but the points are colored according to the different features used to characterize the images. The selected samples are shown in red. It can be noticed that the sampling methodology selects a subset of images that uniformly covers the distribution of the data. Furthermore, as also suggested by the histograms in Figure 7, the sampling was capable of covering the full range of values of every considered feature.

The subset of images selected by the method is shown in Figure 9. The subset indeed contains a heterogeneous set of images covering many different values of the considered features (e.g., low contrast, high vessel density, etc.).

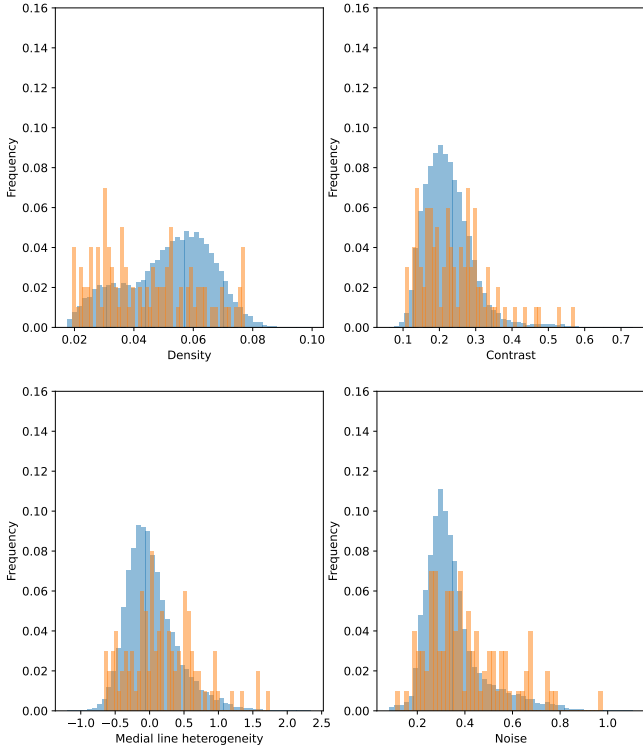


FIG. 7. Histograms of the four features calculated from the blood vessel dataset. Blue bars correspond to the distribution of the full data. Orange bars correspond to the distribution of the sampled subset. Note that the frequencies were normalized by their sum.

This subset can then be manually annotated and used for training a machine learning algorithm to segment the full dataset. Since atypical samples are well-represented, we expect fewer biases in downstream analyses using the obtained segmentation. For instance, some of the samples in the dataset come from animals who suffered hemorrhagic strokes. These samples are very different from the typical samples contained in the dataset, and they would be largely underrepresented if a sampling following the data distribution was performed.

D. Dataset availability

In order to provide a new dataset for training blood vessel segmentation algorithms, we manually labeled each of the 100 images sampled using our method and made the dataset publicly available ². To account for inter-annotator variability, 20 samples were labeled by two annotators. The repository includes manually annotated binary labels, their skeletons (calculated by the

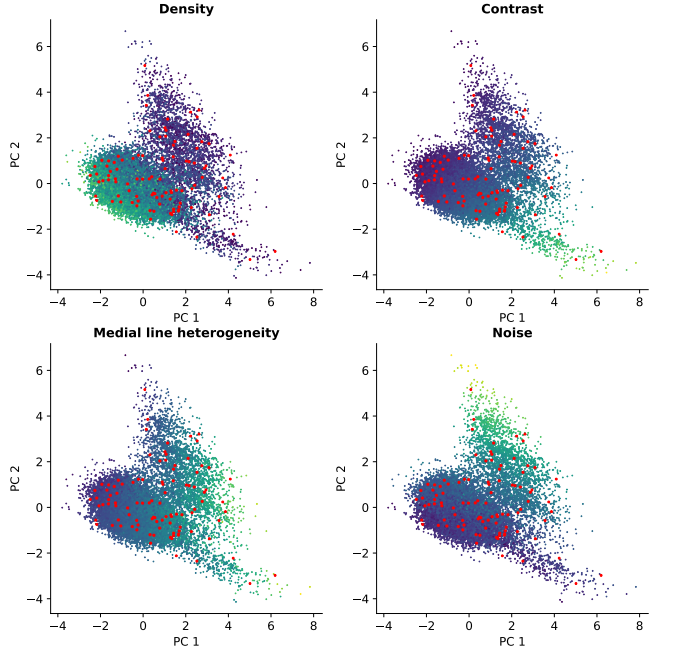


FIG. 8. PCA of the blood vessel dataset. The original features with z-score normalization was used. Red points correspond to the sampled subset obtained by the sampling methodology. Other points correspond to the unselected points, with their colors representing the value of each one of the four original metrics: vessel density, contrast, medial line heterogeneity, and image noise.

Palágyi-Kuba algorithm [29]), and the metrics for each sample (as described in section III B) – which were calculated using the manual annotations. We verified that the metrics calculated from the manual annotations have a strong correlation with the metrics calculated using the labels obtained from the semi-supervised segmentation algorithm. This evidences the quality of the algorithm in providing useful metrics to map the dataset into a feature space. We expect the VessMAP Dataset to be useful for future studies regarding the influence of image and tissue characteristics on the generalization capability of segmentation algorithms.

IV. CONCLUSION

Selecting appropriate images from a larger dataset for training machine learning algorithms is an important task that has been given relatively little attention. This is because the usual approach is to use as many images as possible. While this approach is relevant for general classification problems, for medical image segmentation, where image annotation can be very costly, the images used must be carefully selected in order to ensure good coverage of different tissue appearances and imaging variations. In addition, it is important that the selected images do not lead to biases in downstream tasks related

² VessMAP (Feature-Mapped Cortex Vasculature Dataset): <https://doi.org/10.5281/zenodo.10045265>

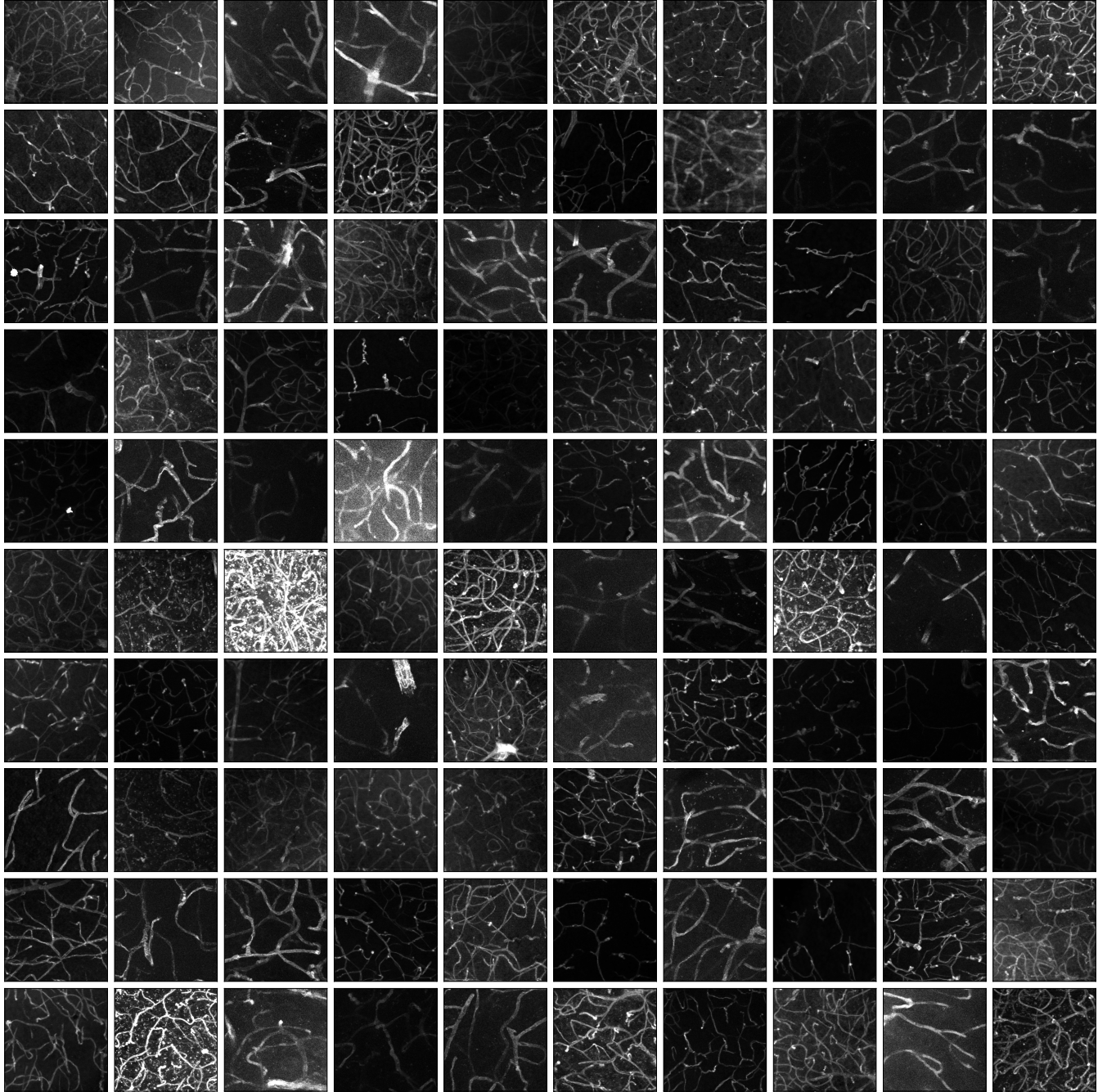


FIG. 9. Subset obtained by our methodology. The images cover a wide range of values in the feature space defined by our four features. Contrast variation and vessel density are the easier features to visually verify. Medial line heterogeneity can be verified by how much the brightness changes longitudinally within a blood vessel. Gaussian noise level is harder to verify visually, but pronounced noise can be observed on some of the brighter images.

to tissue characterization. For instance, we argued that training segmentation algorithms mostly on prototypical images can lead to incorrect measurements on samples having unusual properties (e.g., very bright or very noisy).

We developed an intuitive sampling methodology that evenly selects, as best as possible, both typical and atyp-

ical samples for creating a rich dataset that can then be annotated and used for training segmentation algorithms. One important property of the method is that it provides an intuitive uniform grid in the feature space that can be used for further analyses. For example, one can study the accuracy of the segmentation on different regions of the grid to identify regions where samples

are not being correctly segmented. A robust algorithm should provide good segmentation no matter if a sample is too noisy, bright or dark, if it has low or high contrast or any other variation on relevant image properties. Likewise, expected tissue changes in the samples should not lead to variations in accuracy.

The method has only two parameters, the resolution and the radius of the hyperspherical structuring element. The resolution can be set according to the scale in the feature space where images become too similar, and thus there is no need to consider multiple images with such small variations in appearance. The radius of the hypersphere can be adjusted according to the average distance between points in the dataset. For instance, one can calculate the average distance between the nearest neighbors for each point in the dataset to gain intuition about the typical distances involved and then set the radius as a multiple of this distance.

We applied the methodology to a blood vessel dataset and showed that it can generate a heterogeneous set of samples representing many possible variations of image noise and contrast as well as blood vessel density and intensity variance. A segmentation algorithm that can successfully identify the blood vessels on the selected images should generalize well on the whole dataset. More impor-

tantly, the selected samples guarantee that the algorithm will not focus only on the most prototypical samples, which reduces the chances of biases in the segmentation.

While the methodology was presented focusing on sample selection for annotation, it can also be used on any dataset to analyze possible performance biases of machine learning algorithms. For instance, one could define an appropriate latent space for the ImageNet [30] and generate a subset of samples that uniformly covers the space. The performance of a robust classifier should be similar in all regions of this space. Therefore, the sampling methodology presented here can also be used for interpreting so-called *black box* machine learning algorithms [31].

FUNDING

Cesar H. Comin thanks FAPESP (grant no. 21/12354-8) for financial support. The authors acknowledge the support of the Government of Canada’s New Frontiers in Research Fund (NFRF) (NFRFE-2019-00641) and Google’s Latin America Research Awards (LARA 2021).

- [1] Lei Cai, Jingyang Gao, and Di Zhao, “A review of the application of deep learning in medical image classification and segmentation,” *Ann Transl Med* **8**, 713 (2020).
- [2] Leiyu Chen, Shaobo Li, Qiang Bai, Jing Yang, Sanlong Jiang, and Yanming Miao, “Review of image classification algorithms based on convolutional neural networks,” *Remote Sensing* **13** (2021), 10.3390/rs13224712.
- [3] Zhuang Liu, Hanzi Mao, Chao-Yuan Wu, Christoph Feichtenhofer, Trevor Darrell, and Saining Xie, “A convnet for the 2020s,” in *Proceedings of the IEEE/CVF conference on computer vision and pattern recognition* (2022) pp. 11976–11986.
- [4] Ze Liu, Han Hu, Yutong Lin, Zhuliang Yao, Zhenda Xie, Yixuan Wei, Jia Ning, Yue Cao, Zheng Zhang, Li Dong, *et al.*, “Swin transformer v2: Scaling up capacity and resolution,” in *Proceedings of the IEEE/CVF conference on computer vision and pattern recognition* (2022) pp. 12009–12019.
- [5] Kaiming He, Georgia Gkioxari, Piotr Dollar, and Ross Girshick, “Mask r-cnn,” in *Proceedings of the IEEE International Conference on Computer Vision (ICCV)* (2017).
- [6] Nicolas Carion, Francisco Massa, Gabriel Synnaeve, Nicolas Usunier, Alexander Kirillov, and Sergey Zagoruyko, “End-to-end object detection with transformers,” in *European conference on computer vision* (Springer, 2020) pp. 213–229.
- [7] Syed Sahil Abbas Zaidi, Mohammad Samar Ansari, Asra Aslam, Nadia Kanwal, Mamoon Asghar, and Brian Lee, “A survey of modern deep learning based object detection models,” *Digital Signal Processing* **126**, 103514 (2022).
- [8] Enze Xie, Wenhui Wang, Zhiding Yu, Anima Anandkumar, Jose M. Alvarez, and Ping Luo, “Segformer: Simple and efficient design for semantic segmentation with transformers,” in *Advances in Neural Information Processing Systems*, Vol. 34, edited by M. Ranzato, A. Beygelzimer, Y. Dauphin, P.S. Liang, and J. Wortman Vaughan (Curran Associates, Inc., 2021) pp. 12077–12090.
- [9] Shervin Minaee, Yuri Boykov, Fatih Porikli, Antonio Plaza, Nasser Kehtarnavaz, and Demetri Terzopoulos, “Image segmentation using deep learning: A survey,” *IEEE Transactions on Pattern Analysis and Machine Intelligence* **44**, 3523–3542 (2022).
- [10] Ian Goodfellow, Yoshua Bengio, and Aaron Courville, *Deep Learning* (MIT Press, 2016) <http://www.deeplearningbook.org>.
- [11] Suprosanna Shit, Johannes C. Paetzold, Anjany Sekuboyina, Andrey Zhylka, Ivan Ezhov, Alexander Unger, Josien P. W. Pluim, Giles Tetteh, and Bjoern H. Menze, “cldice - a topology-preserving loss function for tubular structure segmentation.” *CoRR* **abs/2003.07311** (2020).
- [12] Agata Mosinska, Pablo Marquez-Neila, Mateusz Kozinski, and Pascal Fua, “Beyond the pixel-wise loss for topology-aware delineation,” in *Proceedings of the IEEE conference on computer vision and pattern recognition* (2018) pp. 3136–3145.
- [13] Matheus V. da Silva, Julie Ouellette, Baptiste Lacoste, and Cesar H. Comin, “An analysis of the influence of transfer learning when measuring the tortuosity of blood vessels,” *Computer Methods and Programs in Biomedicine* **225**, 107021 (2022).
- [14] Ahmad Chaddad, Jihao Peng, Jian Xu, and Ahmed Bouridane, “Survey of explainable ai techniques in healthcare,” *Sensors* **23** (2023), 10.3390/s23020634.

[15] Rodrigo de P. Mendes, Xin Yuan, Elizabeth M. Genega, Xiaoyin Xu, Luciano da F. Costa, and Cesar H. Comin, “Gland context networks: A novel approach for improving prostate cancer identification,” *Computerized Medical Imaging and Graphics* **94**, 101999 (2021).

[16] Julián Pérez-Beteta, David Molina-García, José A. Ortiz-Alhambra, Antonio Fernández-Romero, Belén Luque, Elena Arregui, Manuel Calvo, José M. Borrás, Bárbara Meléndez, Ángel Rodríguez de Lope, Raquel Moreno de la Presa, Lidia Iglesias Bayo, Juan A. Barcia, Juan Martino, Carlos Velásquez, Beatriz Asenjo, Manuel Benavides, Ismael Herruzo, Antonio Revert, Estanislao Arana, and Víctor M. Pérez-García, “Tumor surface regularity at mr imaging predicts survival and response to surgery in patients with glioblastoma,” *Radiology* **288**, 218–225 (2018), pMID: 29924716, <https://doi.org/10.1148/radiol.2018171051>.

[17] Johannes C. Paetzold, Julian McGinnis, Suprosanna Shit, Ivan Ezhov, Paul Büschl, Chinmay Prabhakar, Anjany Sekuboyina, Mihail Todorov, Georgios Kaassis, Ali Ertürk, Stephan Günemann, and bjoern menze, “Whole brain vessel graphs: A dataset and benchmark for graph learning and neuroscience,” in *Thirty-fifth Conference on Neural Information Processing Systems Datasets and Benchmarks Track (Round 2)* (2021).

[18] Moises Freitas-Andrade, Cesar H. Comin, Matheus Viana da Silva, Luciano F. Fontoura Da Costa, and Baptiste Lacoste, “Unbiased analysis of mouse brain endothelial networks from two- or three-dimensional fluorescence images,” *Neurophotonics* **9**, 031916 (2022).

[19] Alice Krestanova, Jan Kubicek, and Marek Penhaker, “Recent techniques and trends for retinal blood vessel extraction and tortuosity evaluation: A comprehensive review,” *Ieee Access* **8**, 197787–197816 (2020).

[20] Annika Reinke, Minu D. Tizabi, Carole H. Sudre, Matthias Eisenmann, Tim Rädsch, Michael Baumgartner, Laura Acion, Michela Antonelli, Tal Arbel, Spyridon Bakas, Peter Bankhead, Arriel Benis, M. Jorge Cardoso, Veronika Cheplygina, Evangelia Christodoulou, Beth Cimini, Gary S. Collins, Keyvan Farahani, Bram van Ginneken, Ben Glocker, Patrick Godau, Fred Hamprecht, Daniel A. Hashimoto, Doreen Heckmann-Nötzel, Michael M. Hoffman, Merel Huisman, Fabian Isensee, Pierre Jannin, Charles E. Kahn, Alexandros Karargyris, Alan Karthikesalingam, Bernhard Kainz, Emre Kavur, Hannes Kenngott, Jens Kleesiek, Thijs Kooi, Michal Kozubek, Anna Kreshuk, Tahsin Kurc, Bennett A. Landman, Geert Litjens, Amin Madani, Klaus Maier-Hein, Anne L. Martel, Peter Mattson, Erik Meijering, Björn Menze, David Moher, Karel G. M. Moons, Henning Müller, Brennan Nichyporuk, Felix Nickel, M. Ali- can Noyan, Jens Petersen, Gorkem Polat, Nasir Rajpoot, Mauricio Reyes, Nicola Rieke, Michael Riegler, Hassan Rivaz, Julio Saez-Rodriguez, Clarisa Sanchez Gutierrez, Julien Schroeter, Anindo Saha, Shravya Shetty, Maarten van Smeden, Bram Stieljes, Ronald M. Summers, Abd el A. Taha, Sotirios A. Tsaftaris, Ben Van Calster, Gaël Varoquaux, Manuel Wiesenfarth, Ziv R. Yaniv, Annette Kopp-Schneider, Paul Jäger, and Lena Maier-Hein, “Common limitations of image processing metrics: A picture story,” (2021).

[21] Agrim Gupta, Piotr Dollár, and Ross Girshick, “Lvis: A dataset for large vocabulary instance segmentation,” (2019), arXiv:1908.03195 [cs.CV].

[22] Chengcheng Guo, Bo Zhao, and Yanbing Bai, “Deepcore: A comprehensive library for coreset selection in deep learning,” in *Database and Expert Systems Applications*, edited by Christine Strauss, Alfredo Cuzzocrea, Gabriele Kotsis, A. Min Tjoa, and Ismail Khalil (Springer International Publishing, Cham, 2022) pp. 181–195.

[23] Hao Zheng, Lin Yang, Jianxu Chen, Jun Han, Yizhe Zhang, Peixian Liang, Zhuo Zhao, Chaoli Wang, and Danny Z Chen, “Biomedical image segmentation via representative annotation,” in *Proceedings of the AAAI Conference on Artificial Intelligence*, Vol. 33 (2019) pp. 5901–5908.

[24] Bishwo Adhikari, Esa Rahtu, and Heikki Huttunen, “Sample selection for efficient image annotation,” in *2021 9th European Workshop on Visual Information Processing (EUVIP)* (2021) pp. 1–6.

[25] Baptiste Lacoste, Cesar H. Comin, Ayal Ben-Zvi, Pascal S. Kaeser, Xiaoyin Xu, Luciano da F. Costa, and Chenghua Gu, “Sensory-related neural activity regulates the structure of vascular networks in the cerebral cortex,” *Neuron* **83**, 1117–1130 (2014).

[26] Ayden Gouveia, Matthew Seegobin, Timal S. Kannangara, Ling He, Fredric Wondisford, Cesar H. Comin, Luciano da F. Costa, Jean-Claude Béique, Diane C. Lagace, Baptiste Lacoste, and Jing Wang, “The apk-cbp pathway regulates post-stroke neurovascular remodeling and functional recovery,” *Stem Cell Reports* **9**, 1735–1744 (2017).

[27] Julie Ouellette, Xavier Toussay, Cesar H. Comin, Luciano da F. Costa, Mirabelle Ho, María Lacalle-Auriolés, Moises Freitas-Andrade, Qing Yan Liu, Sonia Leclerc, Youlian Pan, Ziyi Liu, Jean-François Thibodeau, Melissa Yin, Micael Carrier, Cameron J. Morse, Peter Van Dyken, Christopher J. Bergin, Sylvain Baillet, Christopher R. Kennedy, Marie-Ève Tremblay, Yannick D. Benoit, William L. Stanford, Dylan Burger, Duncan J. Stewart, and Baptiste Lacoste, “Vascular contributions to 16p11.2 deletion autism syndrome modeled in mice,” *Nature Neuroscience* **23**, 1090–1101 (2020).

[28] David L Donoho and Iain M Johnstone, “Ideal spatial adaptation by wavelet shrinkage,” *Biometrika* **81**, 425–455 (1994), <https://academic.oup.com/biomet/article-pdf/81/3/425/26079146/81.3.425.pdf>.

[29] Kàlmàn Palàgyi and Attila Kuba, “A 3d 6-subiteration thinning algorithm for extracting medial lines,” *Pattern Recognition Letters* **19**, 613–627 (1998).

[30] J. Deng, W. Dong, R. Socher, L.-J. Li, K. Li, and L. Fei-Fei, “ImageNet: A Large-Scale Hierarchical Image Database,” in *CVPR09* (2009).

[31] Cynthia Rudin, “Stop explaining black box machine learning models for high stakes decisions and use interpretable models instead,” *Nature Machine Intelligence* **1**, 206–215 (2019).